ORIENTAL JOURNAL OF CHEMISTRY
An International Open Access, Peer Reviewed Research Journal
www.orientjchem.org
ISSN: 0970-020 X
CODEN: OJCHEG
2025, Vol. 41, No.(2):
Pg. 356-363

Application of Box-Behnken Design for Optimizing the Removal of Penicillin G of Phar-maceutical Wastewater in the Photocatalytic Process with $CoFe_2O_4$@3DTiO_2-doped Po-rous Graphene Aerogel

ZOHREH POOZESH[1], SHAYAN RAHIMI[2], MARYAM RASTEGAR[3], ALI MESHKINIAN,[4] DAVOUD BALARAK*[5] and SHAZIYA HASEEB SIDDIQUI[6]

[1]Department of Pharmacy, Isfahan University of Medical Siences, Isfahan, Iran.
[2]University of Southern California: Los Angeles, California, US.
[3]Department of Pharmaceuticals Chemistry, Shiraz university of technology, Shiraz, Iran.
[4]Department of Occupational Health Engineering, Health Promotion Research Center, Zahedan University of Medical Sciences, Zahedan, Iran.
[5]Department of Environmental Health Engineering, Health Promotion Research Center, Zahedan University of Medical Sciences, Zahedan, Iran.
[6]Department of Chemistry, Sam Higginbottom University of Agriculture Technology and Sciences (SHUATS), Allahabad, Uttar Pradesh, India.
*Corresponding author E-mail: dbalarak2@gmail.com

http://dx.doi.org/10.13005/ojc/410203

(Received: January 27, 2024; Accepted: March 13, 2025)

ABSTRACT

The presence of antibiotics in water sources is a critical concern for public health and envi-ronmental safety worldwide. This research investigates the application of $CoFe_2O_4$@three-dimensional-TiO_2 within a hierarchical porous graphene aerogel (C3DTHPGA), aiming to optimize the removal of Penicillin G (PG) from water. A total of 17 degradation experiments were carried out based on recommendations from a statistical tool using Design Expert 9.0 software. The structural characteristics of C3DTHPGA were examined using SEM, FTIR, and BET techniques. The specific surface area, total pore volume, and pore diameter of the sample derived from tea waste C3DTHPGA were found to be 95.2 m^2/g, 0.12 cm^3/g, and 12 nm, respectively, indicating a strong potential for enhanced PG adsorption. The results fit well into a quadratic model, showing a significant p-value of 0.0109 and a high determination coefficient (R^2) of 0.991. Optimization through Response Surface Methodology (RSM) achieved a peak PG removal efficiency of 99.5% under optimal conditions involving an initial PG concentration of 50 mg/L, a catalyst weight of 0.6 g, and a contact time of 60 minutes. These outcomes underscore the effectiveness and sustainability of C3DTHPGA as a catalyst for reducing PG contamination in water.

Keywords: Penicillin G, C3DTHPGA, Photocatalytic process, RSM-BBD. Determination coefficient.

INTRODUCTION

To improve quality of life, pharmaceuticals and antibiotics are utilized.[1] These antibiotics serve as crucial antimicrobial agents for treating diseases in humans and animals.[2] The widespread presence of pharmaceuticals in the environment is now acknowledged as a global issue.[3] Due to their ongoing discharge and persistence, even at minimal concentrations, they are categorized as emerging contaminants (EC).[4]

Pharmaceutical companies generate highly concentrated antibiotic wastewater, which is then discharged into the environment.[5] A significant concentration of ciprofloxacin (31 mg/L) has been observed in wastewater from ten pharmaceutical manufacturers. Studies indicate that wastewater from the pharmaceutical industry contains higher levels of antibiotic resistance genes compared to municipal wastewater.[6] These contaminants have been found globally in surface waters, drinking waters, wastewater effluents, and soils.[7] Following digestion and metabolism within the body, residues of these substances and their metabolites enter the environment through human excreta.[8,9] The proliferation of antibiotic-resistant microbes in the environment is recognized worldwide as a critical public health concern, raising questions about our future capacity to manage infectious diseases.[10,11] Antibiotics can alter the microbial populations within a wastewater system, inhibiting bacteria that break down organic matter.[12]

Various techniques exist for removing pharmaceutical compounds, including adsorption by activated carbon, reverse osmosis, air stripping, and biological methods.[13] However, these methods do not eliminate contaminants; they merely transfer them from one phase to another.[14] Advanced oxidation processes (AOPs) prove beneficial by using hydroxyl radicals to oxidize resistant compounds, transforming them into innocuous products like H_2O and CO_2.[15] Nanophotocatalytic systems are capable of oxidizing antibiotics and transforming them into less toxic by-products or even harmless compounds.[16] TiO_2 is favored due to its high photocatalytic efficiency, non-toxicity, stability in aqueous solutions, and relatively low cost, making it an effective alternative to other methods.[17]

In the realm of photocatalysis, the development of efficient and sustainable catalysts is crucial for advancing applications such as water splitting, pollutant degradation, and energy conversion.[18] One innovative catalyst that has garnered attention is C3DTHPGA. This composite material leverages the synergistic properties of its components to enhance photocatalytic performance.[19] $CoFe_2O_4$, or cobalt ferrite, is a magnetic spinel structure known for its stability and ability to facilitate charge separation due to its intrinsic magnetic properties. This makes it an excellent candidate for use in photocatalytic processes where efficient charge separation is essential to prevent recombination of electron-hole pairs generated during light absorption.[20] The incorporation of $CoFe_2O_4$ into a three-dimensional TiO_2 matrix further enhances its functionality. Titanium dioxide (TiO_2) is a widely studied photocatalyst due to its strong oxidizing power, non-toxicity, and chemical stability under UV light irradiation.[19] By forming a composite with $CoFe_2O_4$, the TiO_2 matrix benefits from improved electron transport pathways and enhanced surface area, which contribute to more effective light absorption and increased active sites for catalytic reactions.[20]

Moreover, embedding this composite into a hierarchical porous graphene aerogel introduces additional advantages. Graphene aerogels are known for their exceptional electrical conductivity, high surface area, and mechanical strength.[18] The hierarchical porosity ensures efficient mass transfer and provides ample space for reactant diffusion, which is critical in maintaining high reaction rates in photocatalytic applications.[19] The synergistic effect of combining $CoFe_2O_4$ with three-dimensional TiO_2 in a graphene aerogel framework results in several key benefits: enhanced light absorption across a broader spectrum due to the presence of multiple components that can absorb different wavelengths; improved charge separation efficiency facilitated by the magnetic properties of $CoFe_2O_4$ and conductive nature of graphene; and increased catalytic activity stemming from the large surface area and accessible active sites provided by the porous structure.[20] In summary, C3DTHPGA represents an advanced photocatalyst design that effectively harnesses the unique properties of each component. This composite material not only improves the efficiency of photocatalytic processes but also opens up new avenues for designing multifunctional catalysts tailored for specific environmental and energy-related applications.[19]

The Box-Behnken design is a popular and efficient experimental design technique used in

Response Surface Methodology (RSM) for optimizing processes and systems by understanding the relationship between multiple independent variables (factors) and a dependent variable (response).[21] At these methods Each factor is studied at three levels: low (-1), middle (0), and high (+1). Each factor level combination appears an equal number of times.[22] Unlike full factorial designs, Box-Behnken doesn't test all possible factor combinations, leading to fewer experiments.[23] It efficiently explores the interactions between factors, which is crucial for optimal process understanding. This design handles multiple factors (3-7 factors are common) effectively.[24]

In this study, we developed a new catalyst for removing the antibiotic PG from aqueous solutions. We also optimized three parameters using a design approach, and ultimately, the degradation mechanism was determined.

MATERIALS AND METHODS

All materials were purchased from Sigma Aldrich. The catalyst was prepared according to the study of Zisti *et al.,*[24] and Fig. 1. The catalyst was extensively analyzed through a range of techniques. FTIR spectroscopy was employed to detect the functional groups present in the studied catalyst. The morphology of catalyst was examined using SEM and TEM.

Box-Behnken Design Concept

The BBD, is a statistical method widely used in response surface methodology (RSM) for process optimization. This design applies a quadratic equation to model the relationship between experimental variables and their responses.[25] A design matrix with three factors and three levels (-1, 0, +1) was created using Design Expert® software. This approach was selected because it minimizes the number of experimental trials compared to other RSM techniques, making it an efficient tool for parameter optimization. Studies have confirmed the effectiveness of the Box-Behnken Design in optimizing the degradation of PG, emphasizing its suitability for similar optimization processes.[26] The levels and ranges of the factors were determined based on preliminary investigations and are shown in coded form in Table 1. RSM was employed to investigate the factors affecting dye removal efficiency (%). A quadratic polynomial model was used to evaluate the influence of the mass of catalyst (A), PG concentration (B), and contact time (C) on the PG removal percentage (R%). A total of 17 experiments were performed, with variables (A), (B), and (C) adjusted according to the design matrix shown in Table 1. This table provides a comparison between the experimental results and the predicted values for PG removal efficiency (R%).

Table 1: Experimental design levels for various parameters

Independent variables	Symbol	Unit	Coded levels				
			α–	– 1	0	+1	+αα
Catalyst dose	A	min	15	30	45	60	90
Concentration	B	g/L	0.2	0.4	0.6	0.8	1
Contact time	C	mg/L	10	25	50	75	100

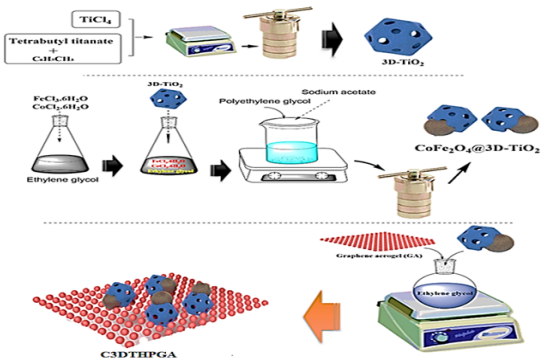

Fig. 1. Synthesis of C3DTHPGA nanocomposite

RESULTS AND DISCUSSION

The synthesized material, C3DTHPGA, demonstrated Type IV nitrogen adsorption-desorption isotherms as shown in Fig. 2a. This suggests that the material features mesoporous properties with relatively sizable pores. The BET analysis revealed a surface area of 95.2 m^2/g and a pore volume of 0.12 cm^3/g. The average pore size was identified to be 12 nanometers, according to the pore size distribution charts in the same figure. In Fig. 2b, the FTIR spectra of the main nanocomposite are presented. The peak at 3435 cm^{-1} is attributed to the vibrations of O-H bonds in water molecules within the sample. Absorption peaks at 1681 and 1082 cm^{-1} are due to the stretching vibrations of the C=O bond.[27] Peaks at 1351 and 1402 cm^{-1} are linked to the stretching vibrations of C–H and C–OH bonds, respectively. Analysis of $CoFe_2O_4$ spectra shows peaks at 468 and 554 cm^{-1}, which are associated with metal stretching vibrations in tetrahedral and octahedral sites, respectively.[28] The interaction between TiO_2 and GA in the composite results in Fe-O vibrational modes, Ti-O-C vibrational states, and Ti-O-Ti bridging stretches, which collectively

produce a broad absorption at 1000 cm^{-1}, confirming the integration of $CoFe_2O_4$, TiO_2, and GA in the composite structure. TEM and SEM images, shown in Fig. 2c and 2d respectively, further confirm that the composites retain a 3D-TiO_2 structure within a porous GA framework characterized by crumpled and aggregated nanoplates, with $CoFe_2O_4$ and 3D-TiO_2 nanoparticles evenly distributed throughout the GA matrix.

Seventeen degradation experiments were performed under conditions recommended by the Design Expert 9.0 software, with the PG removal efficiencies detailed in Table 2. The data in Table 2 show that the maximum removal efficiency of PG was 99.5%, and the minimum was 36.7%. The effective removal of PG correlated with the characterization findings, which showed a greater number of active sites for photocatalytic activity. Table 3 presents summary statistics for different models, including linear, two-factor interaction (2FI), quadratic, and cubic models. The quadratic model was favored by the software due to its superior sequential F-value and lower p-value. A higher sequential F-value coupled with a lower p-value suggests a model's effectiveness in capturing the variability in responses. Models with a p-value above 0.05 lack sufficient evidence to demonstrate that they adequately capture response variability. Consequently, the 2FI and cubic models were aliased based on their sequential p-values, and the quadratic model was selected after a lack of fit test indicated it was most appropriate. This model demonstrated a higher-order polynomial and an F-value of 0.845, which was lower than that of the linear model, and it had the highest p-value of 0.912, suggesting optimal fit to the data. Additionally, the quadratic model was preferred for its highest determination coefficient, R^2 of 0.987, showing excellent agreement with experimental data. The predicted R^2 of 0.988 was close to the adjusted R^2 of 0.991, confirming the model's accuracy without being overfitted. Equation 1 represents the quadratic model for PG removal efficiency in terms of actual factors.

The purpose of this study was to evaluate the feasibility of using the C3DTGOA nanocomposite for photocatalytic degradation of PG. Sustainability assessments were conducted, revealing a decrease in photocatalytic efficiency of 6.5% after four recycling sessions (Figure 4).

$$PG\ degradation = 31.5 + 6.45\ A + 2.36\ B + 11.2\ C + 1.12\ AC + 0.672\ BC - 0.41\ B^2 - 0.64\ C^2 \quad (1)$$

The impact of initial PG concentration, catalyst weight, and contact time on removal efficiency was explored through three-dimensional surface and contour plots. As illustrated in Fig. 3a-b, an increase in initial PG concentration led to a decrease in removal efficiency due to faster saturation of the adsorbent, thus diminishing its capacity for effective PG ion removal. [28] Conversely, an increase in catalyst weight enhanced removal efficiency by providing more adsorption sites.[29] However, as shown in Fig. 3a and c, beyond an adsorbent weight of 0.6 g, further increases led to reduced efficiency because of particle aggregation, which decreased the availability of active sites.[30] Additionally, enhancements in both initial catalyst concentration and adsorbent weight initially raised removal efficiency due to more available adsorption sites.[31]

The data presented in Fig. 3b-c indicate that an increase in contact time improves removal efficiency, attributed to the presence of more vacant sites and a higher concentration gradient across PG ions.[32] The maximum removal efficiency recorded was 99.2% under the conditions of an initial PG concentration of 50 mg/L, using 0.6 g of adsorbent, and a contact duration of 60 min, as depicted in Fig. 3a-c. Factors such as the initial concentration of PG, the mass of the adsorbent, and the duration of contact are crucial determinants of the efficiency with which PG is removed.

In this investigation, the repeated use of the catalyst across four stages indicated its applicability over multiple cycles (Fig. 4). The observed reduction in removal efficiency during these stages is likely due to the diminished quantity of catalyst retrieved after each cycle. Additionally, the environmental safety of the materials was assessed by measuring the leaching of metal ions post-degradation. Only minimal quantities of Fe and Co ions, specifically 0.41% and 0.56% respectively, were detected, demonstrating the physicochemical robustness of the C3DTGOA degradation system as corroborated by related studies. The findings suggest that the degradation of organic compounds through this method does not lead to secondary pollution.

Figure 5 illustrates a proposed mechanism for the breakdown of PG by the C3DTGOA photocatalyst. To understand this mechanism, it is crucial to first determine the VB and CB potentials of the involved materials.[33] This requires calculations using equations 2 and 3. ECB and EVB represent the CB and VB potentials of the semiconductor, respectively. The term denotes the Mulliken electronegativity of the catalyst, recorded at 5.81 eV for both titanium dioxide and cobalt ferrite. Ec indicates the energy of free electrons (4.5 eV) on the hydrogen scale, while Eg represents the band gap energy of the photocatalyst.[34]

$$E_{CB} = \chi - E_C - 0.5E_g \quad (2)$$

$$E_{VB} = E_{CB} + E_g \quad (3)$$

Based on the E_g values from UV-Vis DRS analysis and prior research, ECB and EVB for cobalt ferrite were calculated as +0.62 eV and +2.0 eV, respectively, and for 3D-titanium dioxide as -0.29 eV and +2.91 eV.[36] Upon exposure to visible light, both 3D-titanium dioxide and cobalt ferrite exhibit excitation from the VB to the CB, generating electrons and holes within these bands. Electrons in the CB of 3D-titanium dioxide swiftly move to the GOA networks, reacting with oxygen molecules to form O_2•-.[37] This step inhibits electron-hole recombination on the surface of 3D-titanium dioxide particles. The remaining holes in the VB of titanium dioxide transform PG into less harmful compounds such as COαand HαO.[38] Additionally, these holes can oxidize water molecules or hydroxide ions to generate •HO radicals, given their higher positive potential relative to the potential of H O/•HO (E_o = + 2.34 eV vs. NHE) and OH^-/•HO (E_o = +1.99 eV vs. NHE).[39] Furthermore, holes in the VB of titanium dioxide can transfer to the VB of cobalt ferrite due to its lower energy potential, promoting effective charge separation and enabling direct decomposition of PG by the VB of cobalt ferrite.[40] Besides these factors, cobalt ferrite also contributes with its strong magnetic properties (71.2 emu/g), enhancing the separation of the photocatalyst post-photocatalysis. Ultimately, the generation of reactive oxygen species, including O_2•- and •OH, alongside holes, facilitates the conversion of PG into various molecular weight products, CO_2, and H_2O.[41,42]

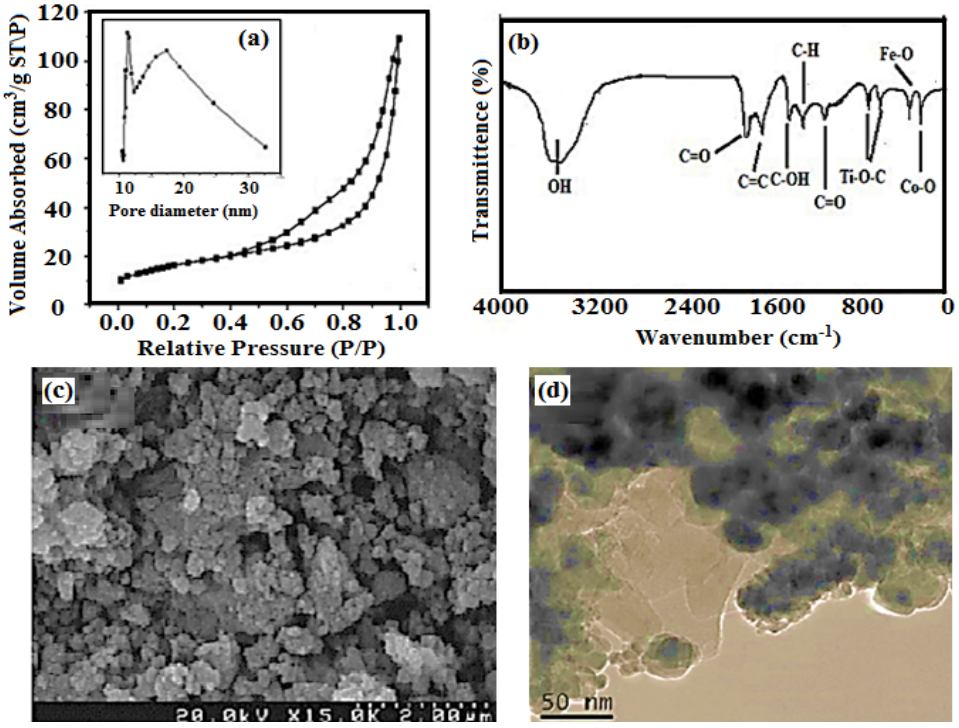

Fig. 2. N_2 adsorption-desorption isotherms (a); FTIR (b); FESEM image (c) and TEM images (d) for C3DTGOA nanocomposite

Table 2: Experimental results and the predicted values of percentage removal

	Parameters			%R	
Run	A	B	C	Experimental	Predicted
1	0.2	10	15	38.3	35.6
2	0.4	10	15	42.3	44.2
3	0.2	25	60	55.2	58.3
4	0.6	25	60	42.1	42.3
5	0.4	10	60	36.4	35.2
6	0.8	50	30	53.2	54.2
7	0.8	50	30	52.4	55.2
8	1	75	30	61.2	60.2
9	1	100	15	42.3	44.2
10	0.6	75	45	63.8	65.3
11	0.8	25	45	73.7	74.2
12	0.4	50	45	58.7	59.3
13	1	25	90	97.1	96.4
14	0.2	10	90	61.3	60.2
15	0.6	75	90	88.9	88.2
16	0.8	75	60	99.5	99.4
17	0.6	50	60	98.9	99.2

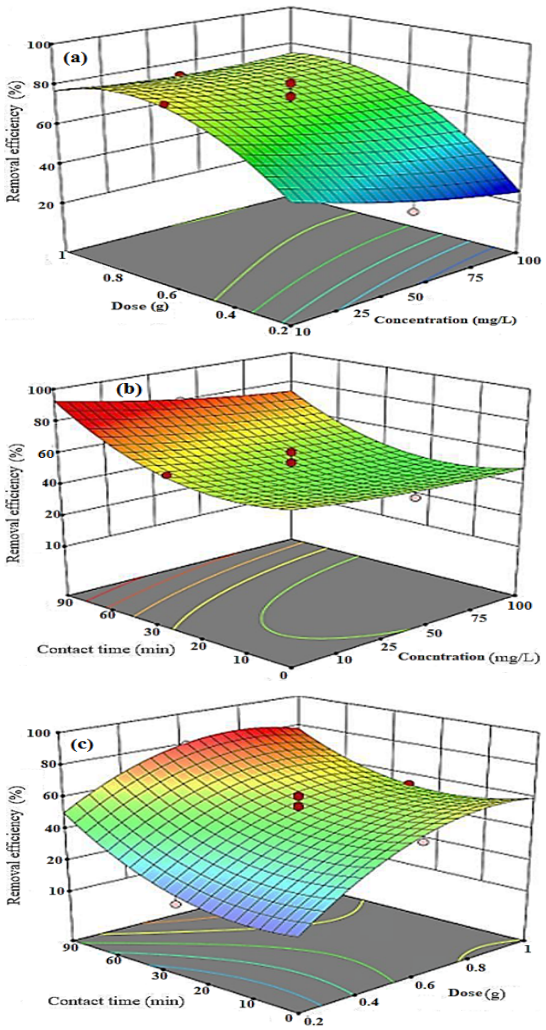

Fig. 3. Three-dimensional surface plot, Contour plot of effects of concentration and dose (a); concentration and contact time (b); dose and contact time (c)

Table 3: Analysis of variance (ANOVA) for PG removal

Source	DF	Pyrocatechol			
	Sum of squares	Mean square	F-value	P-value	
Model	7	8245.1	1745.3	121.2	< 0.0001
A-Contact time	1	985.4	756.3	142.3	< 0.0001
B-dose	1	1235.6	1025.3	189.2	< 0.0001
C-concentration	1	746.2	985.3	145.2	< 0.0001
AB	1	21.7	117.2	3.25	< 0.0001
AC	1	29.2	9.87	1.65	< 0.0001
BC	1	17.3	4.21	2.35	< 0.0001
A^2	1	412.8	7863.8	120.3	< 0.0001
B^2	1	321.3	569.3	189.2	< 0.0001
C^2	1	124.3	472.3	241.2	< 0.0001
R^2		R^2-Adj	R^2-Pred		Adeq Precision
0.987		0.991	0.988		17.21

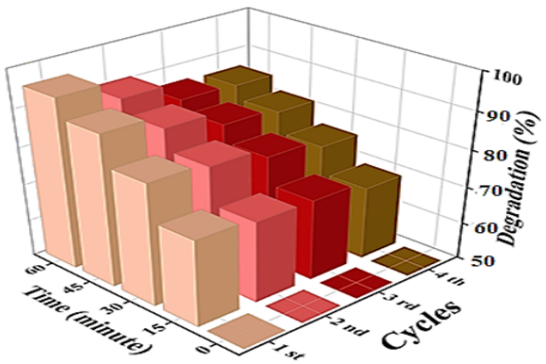

Fig. 4. Catalyst recovery in four cycles for degradation of PG

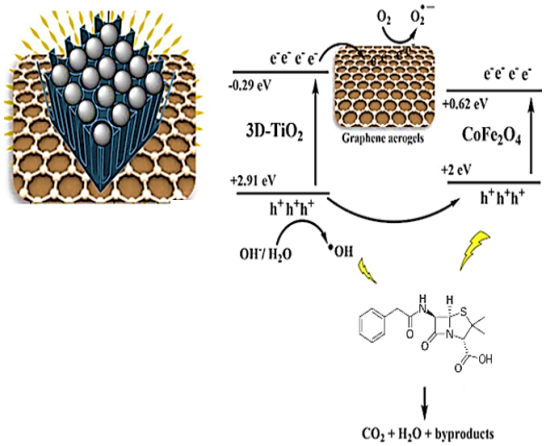

Fig. 5. The possible degradation mechanism of PG based C3DTGOA

CONCLUSION

In this study, the efficiency of the new catalyst (C3DTHPGA) in a photocatalytic process on the removal rate of the antibiotic PG was tested and discussed. Finally, the parameters of contact

time of catalyst dose and PG concentration in a batch process were investigated. In this study, 17 test samples were designed through Design Expert® software. Three-dimensional graphs showed that the removal percentage increased with increasing contact time, catalyst dose, and PG concentration. The optimal conditions of 50 mg/L initial PG concentration, 0.6 g adsorbent weight, and 60 min contact time yielded a PG removal efficiency of 99.5%. Catalyst recovery was successfully performed in 4 steps and the stability of the catalyst was concluded. Finally, it can be concluded that the C3DTHPGA catalyst was able to remove the PG from aqueous environments in a photocatalytic process with an optimal number of experiments.

ACKNOWLEDGEMENT

The authors are grateful from Zahedan University of Medical Sciences, because of supporting of this research.

Conflict of interest

The authors declare that there is no conflict of interest.

Funding

There is no funding in this work.

REFERENCES

1. Zisti F.; Chandrika K.; Balarak D., *Int J Pharm Investigation.*, **2023**, *13*(4), 778-83.
2. Naghsh N.; Barnoos S.; Zisti F.; Chandrika K., *Int J Pharm Investigation.*, **2024**, *14*(2), 365-70.
3. Mostafapour FK.; Haseeb S.; Balarak D.; Moein H.; Sajadi AA.; Jalalzaei Z., *Int J Pharm Investig.*, **2021**, *11*(1), 41-5.
4. Balarak D.; Chandrika K., *Int J Pharm Investig.*, **2019**, *9*(3), 117-21.
5. Gashtasbi F.; Yengejeh RJ. Babaei, A. A., *Korean J. Chem. Eng.,* **2018**, *35*, 1726–1734.
6. Bansal P.; Verma A.; Mehta, C., *J Mater Sci.*, **2018**, *53*, 7326–7343.
7. Bansal P.; Verma A.; Aggarwal K.; Singh A.; Gupta S., *Can J Chem Eng.*, **2016**, *94*, 1269–1276.
8. Ajoudanian N.; Nezamzadeh-Ejhieh A., *Mater Sci Semicond Process.*, **2015**, *36*, 162–169.
9. Moein H.; Balarak D.; Meshkinain A.; Chandrika K.; Yazdani N., *Int J Pharm Investig.,* **2021**, *11*(1), 23-6.
10. Mostafapour FK.; Bazi M.; Siddiqui SH.; Bagheri H., *Int J Pharm Investig.*, **2021**, *11*(4), 384-8.
11. Haw, C., *New J. Chem.*, **2016**, *40*, 1124–1136.
12. Erim B.; Cigeroglu Z.; Bayramoglu M., *J Mol Struct.*, **2021**, *1234*, 130194.
13. Mukhopadhyay S.; Maiti D.; Saha A.; Devi PS., *Cryst Growth Des.*, **2016**, *16*(12), 6922–6932.
14. Malinowska I.; Kubica P.; Madajski, P., *Environ Sci Pollut Res.*, **2022**, *30*, 35929–35944.
15. Liu W.; Du T.; Ru Q.; Zuo S.; Yao C., *Nanotechnol Environ Eng.*, **2018**, *3*(1), 5. https://doi.org/10.1007/s41204-018-0035-1.
16. Dianati.; R.A. Mengelizadeh.; N. Zazouli, M.A., *Inter. J. Environ. Anal. Chem.*, **2022**, *101*, 1-11.
17. Balarak D.; Mengelizadeh N.; Rajiv P.; Chandrika, K., *Environ Sci Pollut Res.*, **2021**, *28*(36), 49743–49754.
18. Bagheri Ghomi A.; Ashayeri V., *Iran. J. Catal.*, **2012**, *2*(3), 135-140.
19. Al-Musawi T.; McKay G.; Rajiv P., *J. Photochem. Photobiol.*, A., **2022**, *424*, 113617.
20. Tavakoli F.; Badiei A.; Yazdian F., *J Clust Sci.*, **2017**, *28*, 2979–2995.
21. Ankita B.; Rakshitha R. & Pallavi, N., *Environ Monit Assess.*, **2024**, *196*, 625.
22. Zulfiqar, M.; Chowdhury, S.; Omar, A. A., *Environ. Sci. Pollut. Res.*, **2020**, *27*, 34018–34036.
23. Rakshitha R.; Rajesh C.; Gurupadayya, B., *Environ. Sci. Pollut. Res.*, **2023**, *30*(30), 75655–67.
24. Zisti F.; Kaur I.; Awad S.A., *Environ Sci Pollut Res.*, **2025**. https://doi.org/10.1007/ s11356-024-35787-1.
25. Shekofteh-Gohari M.; Habibi-Yangjeh A., *RSC Adv.*, **2016**, *6*, 2402–2413.
26. Kulkarni SD.; Kumbar S.; Menon SG.; Choudhari KS., *Mater. Res. Bull.*, **2016**, *77*, 70–77.
27. Balarak D.; Baniasadi M.; Bazzi M., *Int J Pharm Investig.*, **2020**, *10*(3), 339-43.
28. Bazi M.; Balarak D.; Khatibi AD.; Siddiqui SH, Mostafapour FK., *Int J Pharm Investig.*, **2021**, *11*(3), 269-73.
29. Al-Hawary SIS.; Rahimpoor R.; Rahmani A.; Romero-Parra RM.; Ramírez-Coronel AA., *Catalysts.*, **2023**, *13*(2), 411. https://doi.org/10.3390/catal13020411.
30. Balarak D.; Ganji F.; Chandrika K.; Haseeb S., *Int J Pharm Investig.*, **2020**, *10*(2), 122-6.

31. Lv D.; Zhang D.; Liu X.; Liu Z.; Hu L., *Sep. Purif. Technol*., **2016**, *158*, 302–307.
32. Zhu HY.; Jiang R.; Fu YQ.; Li RR., *Appl. Surf. Sci*., **2016**, 369; 1–10.
33. Fawzy A.; Mahanna H.; Mossad M., *Environ Sci Pollut Res*., **2022**, *29*, 68532–68546.
34. Balarak D.; Khatibi AD.; Chandrika K., *Int J Pharm Investig*., **2020**, *10*(2), 106-11.
35. Rezaei, M.; Mengelizadeh, N.; Berizi, Z., *ChemistrySelect.,* **2023**, *8*(2), 10-19.
36. Yilmaz M.; Mengelizadeh N.; Saloot, MK, & shahbaksh, S., *Mater. Sci. Semicond. Process*., **2022**, *144*, 106593.
37. Mohagheghian, A.; Ayagh K.; Godini K and Shirzad-Siboni M., *J. Adv. Oxid. Technol*., **2017**, *20*(2), 11-24.
38. Al-Musawi TJ.; Alghamdi MI.; Alhachami FR., *Environ Monit Assess*., **2023**, *195*, 372.
39. Al-Musawi, TJ.; Rajiv P.; Mengelizadeh N.; Sadat Arghavan F., *J. Mol. Liq*., **2021**, *337*, 116470.
40. Rahimi, Z. Sarafraz.; H. Alahyarizadeh.; G. J. Radioanal., *Nucl. Chem*., **2018**, *317*, 431–442.
41. Li S.; Cai, M.; Wang, C., *Adv. Fiber Mater*., **2023**, *5*, 994–1007.
42. Ahmad, I.; Alshimaysawee, S.; Romero-Parra, R.M., *Environ Sci Pollut Res*., **2023**. https://doi.org/10.1007/s11356-023-29283-1.